DOI: 10.1002/chem.200500540

Controlled Hydrothermal Synthesis of Bismuth Oxyhalide Nanobelts and Nanotubes

Hong Deng, Junwei Wang, Qing Peng, Xun Wang, and Yadong Li*[a]

Abstract: Ternary bismuth oxyhalide crystalline nanobelts (such as $Bi_{24}O_{31}Br_{10}$, Bi_3O_4Br, $Bi_{12}O_{17}Br_2$, BiOCl, and $Bi_{24}O_{31}Cl_{10}$) and nanotubes (such as $Bi_{24}O_{31}Br_{10}$) have been synthesized by using convenient hydrothermal methods. The composition and morphologies of the bismuth oxyhalides could be controlled by adjusting some growth parameters, including reaction pH, time, and temperature. All the nanostructures were characterized by using various methods including X-ray diffraction, transmission electron microscopy, high-resolution TEM, electron diffraction, and energy-dispersive X-ray analysis. The possible reaction mechanism and growth of the crystals are discussed based on the experimental results.

Keywords: bismuth oxyhalides · crystal growth · hydrothermal synthesis · nanobelts · nanotubes

Introduction

Among various nanostructures, one-dimensional (1D) nanostructured materials—such as nanotubes, nanorods, nanowires, and nanobelts—have aroused intense interest because of their potential applications in catalysis, environmentally friendly pigments, building nanodevices, nanosensors, and in fully understanding the dimensionally confined transport phenomena in functional nanomaterials.[1–3] Since the discovery of carbon nanotubes in 1991, considerable strategies have been developed for the growth of novel 1D noncarbon nanostructures, such as metal, transition-metal oxides, halides, chalcogenides, and so forth.[4–7] However, due to a lack of understanding of the general principles of the controlled synthetic processes, up to now only limited types of ternary oxide complexes have been prepared.[8] The exploration for new types of multicomponent 1D nanostructures is still a challenge to scientists.

Bismuth oxyhalides show unique and excellent electrical, magnetic, optical, and luminescent properties, in addition to exhibiting therapeutic modality against microscopic carcinoma and good catalytic activity and selectivity in the oxidative coupling of the methane (OCM) reaction.[9] In general, bismuth halide powders can be prepared by using a hydrolytic method at room temperature. However, the resulting products crystallize relatively poorly. It is known that the physical and chemical properties of materials are strongly dependent on their size, shape, and size distribution.[10] 1D nanostructures of bismuth oxyhalide are of great interest due to their applications in catalysis and their promising properties in the nanometer region. Therefore, the development of convenient strategies for their preparation is deemed necessary. Very recently, we reported a facile, hydrothermal synthetic pathway for the preparation of single-crystalline nanobelts of bismuth oxybromide.[11] Our further studies showed that, by manipulating appropriate reaction parameters such as temperature, time, and pH, ternary bismuth oxychloride nanobelts and bismuth oxybromide nanobelts/nanotubes with different compositions could be selectively synthesized. In this paper, a systematic study has been performed to investigate the controlled synthesis of bismuth oxyhalide nanobelts and nanotubes by adjusting selected growth parameters, and a suitable mechanism has been proposed for their formation.

[a] Dr. H. Deng, Dr. J. Wang, Dr. Q. Peng, Dr. X. Wang, Prof. Dr. Y. Li
Department of Chemistry, Tsinghua University
Beijing, 100084 (P.R. China)
and
National Center for Nanoscience and Nanotechnology
Beijing, 100081 (P.R. China)
Fax: (+86) 10-6278-8765
E-mail: ydli@tsinghua.edu.cn

Supporting information for this article is available on the WWW under http://www.chemeurj.org/ or from the author.

Results and Discussion

Structure and morphology of bismuth oxybromide and oxychloride: Both the literature[4a,b] and our previous stud-

ies[5a,b,c,d] suggest that substances that possess lamellar structures, such as graphite,[4a] WS_2,[4b,5d] and bismuth,[5a] might be able to form nanotubes under favorable conditions. Bismuth oxybromide and oxychloride have a tetragonal $PbFCl^-$-type structure with a space group of *P*4/*nmm*. This is known to be a layered structure, which is constructed by the combination of the halide (bromide or chloride) ion layer and the metal–oxygen (Bi–O) layer as shown in Figure 1.[9a] In our

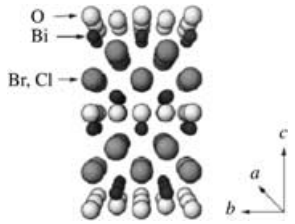

Figure 1. Schematic drawing of the bismuth oxybromide/oxychloride crystal.

opinion, the layered structure of bismuth oxyhalides suggests that nanotubes may be formed under appropriate conditions. Stimulated by the successful synthesis of bismuth nanotubes and nanowires by using a rational low-temperature hydrothermal method,[5a,b] we decided to extend this convenient approach to the fabrication of ternary bismuth oxyhalide nanotubes and nanowires.

The powder X-ray diffraction (XRD) patterns of the as-prepared bismuth halide products are shown in Figures 2

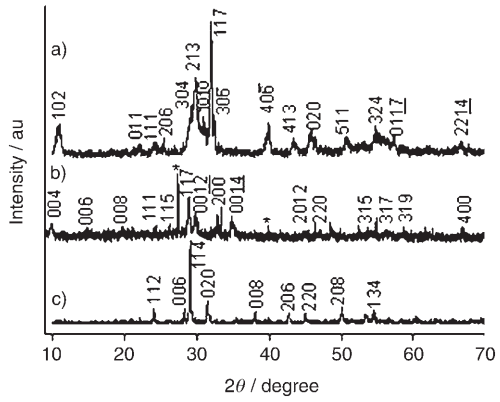

Figure 2. XRD patterns of as-prepared a) $Bi_{24}O_{31}Br_{10}$, b) $Bi_{12}O_{17}Br_2$, and c) Bi_3O_4Br. The * represents peaks of Bi_2O_3.

and 3. Figure 2a shows the monoclinic phase of $Bi_{24}O_{31}Br_{10}$ (JCPDS 75-0888). The XRD pattern of $Bi_{12}O_{17}Br_2$ nanobelts is displayed in Figure 2c; most of the peaks could be indexed to a orthorhombic structure of Bi_3O_4Br (JCPDS 84-0793). Although some peaks assignable to a Bi_2O_3 impurity were also present, all the peaks in Figure 2b could be indexed to a pure tetragonal phase of $Bi_{12}O_{17}Br_2$ (JCPDS 37-0701). The pattern shown in Figure 3a could be readily indexed to the monoclinic phase of $Bi_{24}O_{31}Cl_{10}$ with lattice

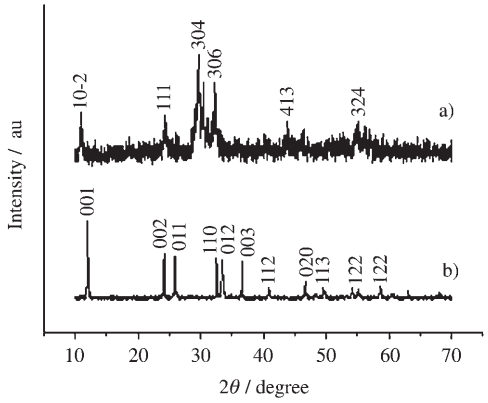

Figure 3. XRD patterns of as-prepared a) BiOCl and b) $Bi_{24}O_{31}Cl_{10}$.

constants of $a=9.99$, $b=3.97$, and $c=6.72$ Å (JCPDS 75-0887), whereas the pattern shown in Figure 3b could be indexed to the tetragonal phase of BiOCl with lattice constants of $a=3.88$ and $c=7.35$ Å (JCPDS No. 73-2060). All these XRD patterns indicated that two different phases of bismuth oxychloride and three different ternary phases of bismuth oxybromide had been successfully synthesized.

Transmission electron microscopy (TEM) provided further insight into the morphological and structural details of these bismuth oxyhalide products. As shown in Figure 4a

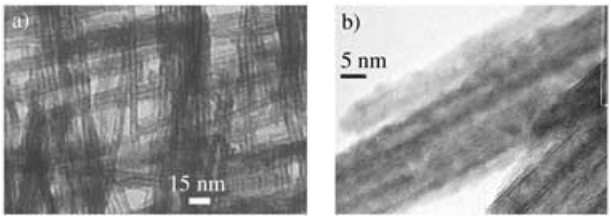

Figure 4. A typical TEM image (a) and a HRTEM image (b) of $Bi_{24}O_{31}Br_{10}$ nanotubes.

and b, $Bi_{24}O_{31}Br_{10}$ samples dispersed on the TEM grids exhibit typical tubular morphology with diameters of 3–8 nm and lengths ranging between 2 and 5 μm. On the other hand, Figure 5a, b, and c illustrates typical TEM images of structurally uniform $Bi_{24}O_{31}Br_{10}$, Bi_3O_4Br, and $Bi_{12}O_{17}Br_2$ nanobelts, respectively. These nanobelts are several micrometers in length and several hundred nanometers in width. The high-resolution transmission electron microscope (HRTEM) image recorded on individual $Bi_{24}O_{31}Br_{10}$ nanobelts (Figure 5d) provided further insight into their structure. The spacing of 0.375 nm between adjacent lattice planes corresponds to the distance between two (008) crystal planes. The selected-area electron diffraction (SAED) pattern (Figure 5e) indicates that the nanobelts are single crystals. Their long axis corresponds to the [001] direction. Energy-dispersive X-ray analyses (EDAX) were carried out to determine the chemical composition of the as-prepared

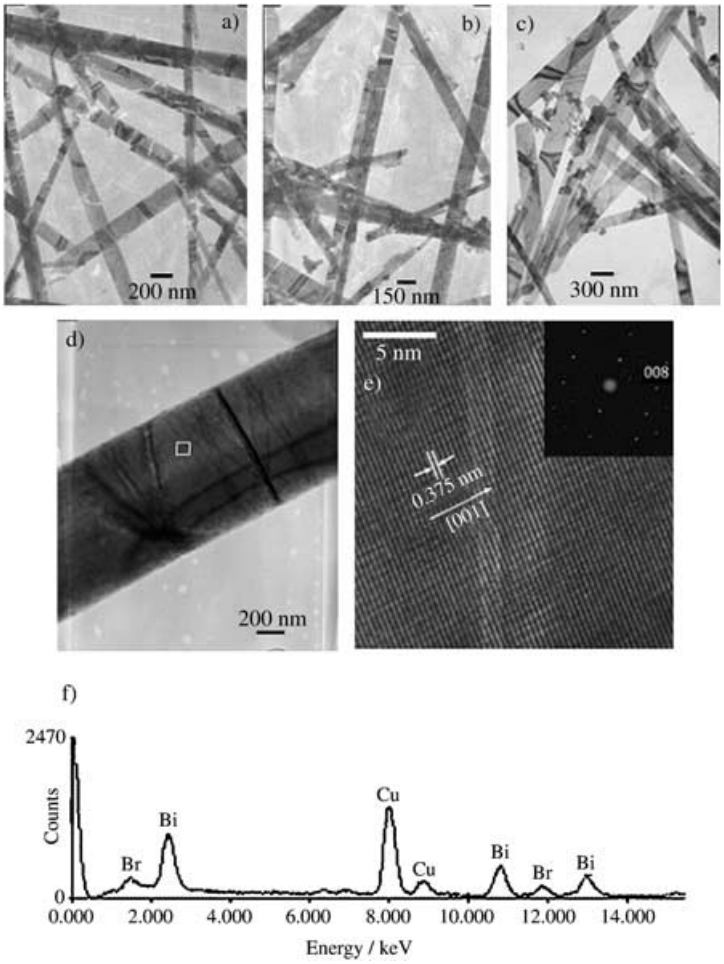

Figure 5. Typical TEM images of a) $Bi_{24}O_{31}Br_{10}$, b) Bi_3O_4Br, and c) $Bi_{12}O_{17}Br_2$ nanobelts, d) HRTEM images of an individual $Bi_{24}O_{31}Br_{10}$ nanobelt, e) a close up of the boxed area in d), and f) an EDXA spectrum of as-prepared $Bi_{24}O_{31}Br_{10}$ nanobelts.

$Bi_{24}O_{31}Br_{10}$ nanobelts (Figure 5f). The EDAX spectra of the $Bi_{24}O_{31}Br_{10}$ nanobelts only show the presence of Bi and Br with a Bi/Br atomic ratio of 2.4:1, which matches their stoichiometries quite well. (The capability of the Hitachi H-800 microscope enables only those elements with atomic numbers greater than Na to be detected; therefore, the O peak was not visible; the Cu signal came from the copper TEM grid).

Figure 6a illustrates uniform BiOCl nanobelts with uniform widths of 100–250 nm and lengths of up to several micrometers. Figure 6b shows a high-resolution TEM image of a single-crystalline BiOCl nanobelt. The SAED pattern (Figure 6b inset) indicates that the nanobelts are single crystals. Their long axis corresponds to the [020] direction. The interlayer distance was calculated to be about 0.28 nm, in good agreement with the separation between the (110) lattice planes. A typical TEM image of as-prepared $Bi_{24}O_{31}Cl_{10}$ exhibiting exclusively beltlike structures is shown in Figure 7a. These nanobelts are long, smooth, and uniform with typical widths in the range of 100–300 nm. A twisted-belt

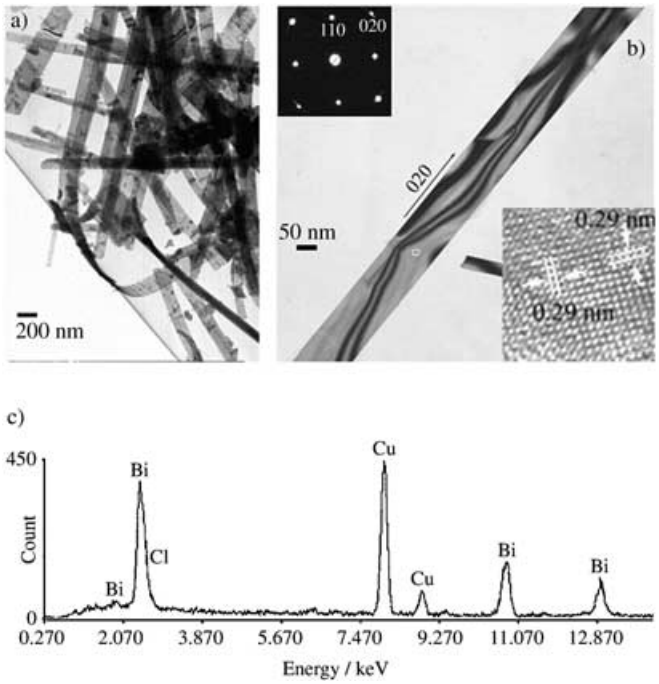

Figure 6. a) A typical TEM image of BiOCl nanobelts with the typical bending morphology, b) a HRTEM image of an individual BiOCl nanobelt, and c) an EDXA spectrum of an individual BiOCl nanobelt.

structure is shown in Figure 7b to demonstrate the beltlike structure. The width-to-thickness ratios are about 8–10 and the thickness of the nanobelts is about 30 nm estimated from the image of twisted nanobelts. EDAX analysis (Figure 6c) on an individual BiOCl nanobelt showed only the presence of Bi and Cl; however, the atom ratio of Bi to Cl could not be determined because one peak for Bi overlapped with the peak for Cl.

Our synthesis is based on the hydrolysis of the bismuth compound at room temperature and the subsequent hydrothermal treatment under designated reaction conditions. By controlling the growth parameters, for example, reaction temperature, time, and pH, bismuth oxyhalide nanobelts or nanotubes could be selectively synthesized in solution.

Influence of the reaction pH: It is generally accepted that the pH of a reaction has great influence on determining the

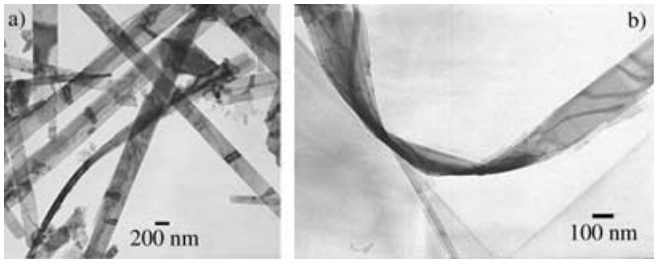

Figure 7. TEM images of a) $Bi_{24}O_{31}Cl_{10}$ nanobelts and b) a twisted $Bi_{24}O_{31}Cl_{10}$ nanobelt.

composition and morphologies of the final products.[12] Control experiments have been carried out to investigate the influence of pH on the reaction. In our experiment, pH also plays a key role in controlling the composition and anisotropic growth of crystals. The results are listed in Table 1. In

Table 1. Bismuth oxyhalides obtained under different reaction conditions.

Sample	Experimental conditions			Morphology
	T [°C]	pH	t [h]	
BiOBr	100–180	1–7	>12	nanoflakes
$Bi_{24}O_{31}Br_{10}$	160–180	8–10	>12	nanobelts
$Bi_{24}O_{31}Br_{10}$	100–120	10	2–4	nanotubes
Bi_3O_4Br	160–180	11–12	>12	nanobelts
$Bi_{12}O_{17}Br_2$	160–180	13–14	>12	nanobelts
BiOCl	160–180	1–7	>12	nanoflakes
BiOCl	160–180	8	>12	nanobelts
$Bi_{24}O_{31}Cl_{10}$	160–180	9–13	>12	nanobelts

general, we prepared $Bi_{24}O_{31}Br_{10}$ nanotubes at pH 10 and nanobelts at pH 8–10; Bi_3O_4Br nanobelts at pH 11–12; $Bi_{12}O_{17}Br_2$ nanobelts at pH 13–14; whereas, BiOBr nanoflakes (see the Supporting Information) were obtained at a lower pH (pH < 7) and Bi_2O_3 microstructures were prepared under more basic (pH > 14) conditions. Due to these basic conditions, Bi_2O_3 product may be present in more than one phase, so to avoid this, vigorous stirring was needed before heating. The possible processes for the formation of $Bi_{24}O_{31}Br_{10}$, Bi_3O_4Br, and $Bi_{12}O_{17}Br_2$ can be described as follows [Eqs. (1)–(4)]:

$$24\,BiOBr + 14\,OH^-_{(aq)} \rightarrow Bi_{24}O_{31}Br_{10} + 14\,Br^- + 7\,H_2O \quad (1)$$

$$Bi_{24}O_{31}Br_{10} + 2\,OH^- \rightarrow 8\,Bi_3O_4Br + 2\,Br^- + H_2O \quad (2)$$

$$4\,Bi_3O_4Br + 2\,OH^- \rightarrow Bi_{12}O_{17}Br_2 + 2\,Br^- + H_2O \quad (3)$$

$$Bi_{12}O_{17}Br_2 + 2\,OH^- \rightarrow 6\,Bi_2O_3 + 2\,Br^- + H_2O \quad (4)$$

From the above equations it can be seen that BiOBr was formed at the beginning of the reaction, then OH^- gradually substituted Br^- in the basic conditions, which resulted in the reduced content of Br^- in the products. In addition, by increasing the pH, $Bi_{24}O_{31}Br_{10}$, Bi_3O_4Br, and $Bi_{12}O_{17}Br_2$ could be gradually obtained. The higher the pH value, the lower the Br^- content in the products, until the content of Br^- in the products was fully replaced by OH^-, finally resulting in the formation of Bi_2O_3 under strong basic conditions. However, BiOBr is the exclusive product from the acidic solution system. Generally, there is a competitive relationship between the OH^- and Br^- ions in basic solution. By controlling the pH of the reaction, different compositions of bismuth oxybromide were obtained.

In order to explore the possibilities of synthesizing new types of nanotubes or nanobelts, we employed our method to the synthesis of bismuth oxychloride nanobelts because of the similar crystal structures and chemical properties of the bromide and chloride bismuth oxyhalides. The beltlike structures of bismuth oxychloride were prepared successfully under similar conditions. The experimental process was the same, except that cetyltrimethyl ammonium chloride (CTAC) was used instead of cetyltrimethyl ammonium bromide (CTAB). Similarly, BiOCl and $Bi_{24}O_{31}Cl_{10}$ nanobelts were obtained at pH 8 and 9–13, respectively. BiOCl nanoflakes (see the Supporting Information) were obtained at lower pH (pH 1–7) and Bi_2O_3 microstructures were obtained under more basic conditions (pH > 14).

Influence of the reaction temperature and time: Layered substances such as graphite can roll up into tubes. It is reasonable to assume that the layers are held together mainly by weak van der Waals forces; this means that by adopting a tubular morphology the energy gap and rigidity would be reduced. Very recently, we synthesized several types of nanotubes from lamellar structures such as WS_2, vanadium oxide, and bismuth.[3a–d] On the basis of our previous studies and the fully demonstrated rolling mechanism, we believed that it should be possible to form 1D nanostructures of bismuth oxyhalide, as nanotubes or nanobelts that have similar layered structures, by choosing appropriate growth conditions. By optimizing the reaction temperature and time, nanotubes and nanobelts of $Bi_{24}O_{31}Br_{10}$ were selectively synthesized. The optimal temperature and time for the growth of the $Bi_{24}O_{31}Br_{10}$ nanotubes were found to be 120 °C and 2–4 h. The optimal temperature and time for the growth of the bismuth oxyhalide nanobelts were 160–180 °C for more than 12 h. If the temperature was lower than this, thermodynamically stable nanoflakes were often obtained. Based on the experimental results, it was reasonable to imagine that at a high reaction pH and low reaction temperature (120 °C) $Bi_{24}O_{31}Br_{10}$ nanotubes would be formed. BiOBr was prepared at first in the initial reaction stages, then OH^- attacked Br^- and gradually substituted it; this may drive the layered structure of $Bi_{24}O_{31}Br_{10}$ into a rolling process and lead to the formation of $Bi_{24}O_{31}Br_{10}$ nanotubes. If the reaction reaches completion, the products keep their tubular structure. Otherwise, if both the reaction temperature and time are increased, the metastable $Bi_{24}O_{31}Br_{10}$ nanotubes collapse, resulting in the formation of more stable nanobelts or nanoflakes. When bismuth oxybromide nanotubes are destroyed by high reaction temperatures it can be expected, based on the "rolling mechanism", that the tubular structure collapses to form nanobelts or unrolls to form large nanoflakes. In addition, this conversion process provides further solid evidence for the "rolling mechanism". From our experiments it was found that a lower temperature favors the formation of nanotubes, while a higher temperature probably leads to the breakdown of rolling process, thus to the formation the more stable nanobelts or nanoflakes. It is worth noting that the conversions among bismuth oxyhalide nanotubes, nanobelts, and nanoflakes raise the possibility that other similarly layered compounds could form nanostructure materials with different morphologies.

Influence of surfactant and bismuth oxyhalide concentration: Other synthetic parameters have also been examined. For example, the surfactant (that is, CTAB or CTAC as the bromide or chloride source, respectively) used to produce the bismuth oxyhalides determines the morphology of the products. Controlled experiments were conducted with the substitution of CTAB by NaBr or CTAC by NaCl, respectively. We found that only BiOBr or BiOCl nanoflakes could be obtained regardless of the pH of the reaction, under otherwise identical conditions. It is believed that the formation of CTA^+OH^- provides appropriate conditions for the growth of nanotubes or nanobelts of bismuth oxybromide or bismuth oxychloride.

With regard to the concentration, nanotubes or nanobelts could be obtained by using a higher concentration of bismuth oxyhalide. It is reasonable to assume that a higher concentration is preferable for the anisotropic growth of crystals, resulting in products with higher aspect ratios. Along with a few nanobelts, large nanoflakes were prepared at a lower concentration, which suggests that low concentration may be of more benefit to the preparation of nanoflakes.

Color and UV-visible absorption spectra: Bismuth oxychloride is an established pigment, with shiny and soft characteristics. It is interesting to note that the bismuth oxychlorides obtained at different pH and with different compositions have different glosses. The color of the products is strongly dependent on their composition and the pH of the reaction environment. With a lower Cl^- content in the product and a higher reaction pH, the color of the samples gradually deepens (from white, to pale yellow, then to yellow, and lastly to deep yellow) from **1** to **4** (Figure 8a), which implies that the intrinsic optical properties have changed. Generally, the color of $Bi_{24}O_{31}Cl_{10}$ is deeper than that of BiOCl. UV-visible absorption experiments were carried out to further investigate the optical properties of these compounds. The absorption spectra of solutions of complexes **1**, **2**, **3**, and **4** in ethanol are given in Figure 8b. The spectra of samples **2**, **3**, and **4** consist of well-resolved bands in the range of 350–550 nm, whereas that of **1** has no obvious UV-visible absorption. The absorption peaks for samples **2**, **3**, and **4** are 390, 392, and 394 nm, respectively, indicating that there is a gradual redshift from compounds **2** to **4**. In addition, the absorption band of each sample gradually became broader and showed the following order (from broadest to less broad): **4** > **3** > **2** > **1**, which is in good agreement with the color change.

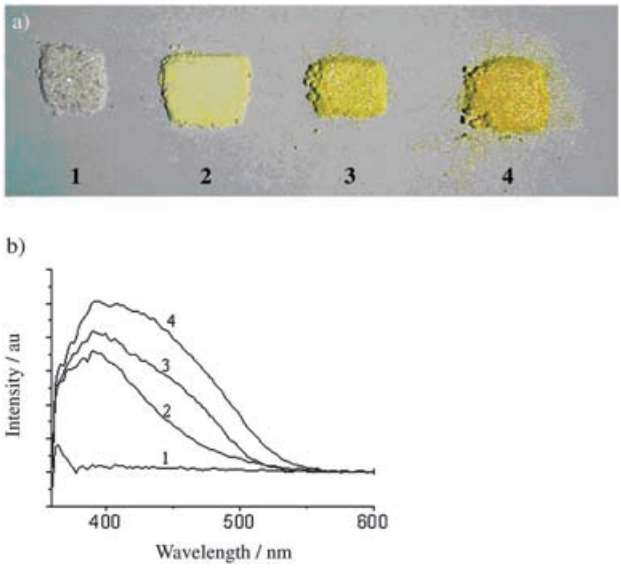

Figure 8. a) Gradual color changes of the as-prepared bismuth oxychloride compounds obtained. BiOCl compounds **1** and **2** were obtained at pH 1 and 3, respectively; $Bi_{24}O_{31}Cl_{10}$ compounds **3** and **4** were obtained at pH 9 and 13, respectively. b) Absorption patterns of BiOCl **1** (pH 1), trace 1; BiOCl **2** (pH 3), trace 2; $Bi_{24}O_{31}Cl_{10}$ **3** (pH 9), trace 3; $Bi_{24}O_{31}Cl_{10}$ **4** (pH 13), trace 4.

Conclusion

In summary, a convenient and controllable hydrothermal method has been developed for the preparation of ternary bismuth oxychloride nanobelts and bismuth oxybromide nanobelts or nanotubes with different compositions by simply changing the pH and temperature. The optimal reaction conditions for the growth of the $Bi_{24}O_{31}Br_{10}$ nanotubes were found to be pH 10 at 120 °C for 2–4 h, whereas those for $Bi_{24}O_{31}Br_{10}$ nanobelts were pH 8–10 at 160–180 °C for more than 12 h; the optimal reaction conditions for the growth of the $Bi_3O_4Br_{10}$ nanobelts were pH 11–12 at 160–180 °C, and those for $Bi_{12}O_{17}Br$ nanobelts were pH 13–14 at 160–180 °C. For reaction times longer than 12 h, the optimal reaction conditions for the growth of the BiOCl nanobelts were found to be pH 8 at 160–180 °C, and those for the $Bi_{24}O_{31}Cl_{10}$ nanobelts were pH 9–13 at 160–180 °C. Generally, lower temperature and shorter reaction time are beneficial for the formation of metastable nanotubes, higher temperature and longer reaction time are preferable for the preparation of the more stable nanobelts or nanoflakes. We believe that this method could also provide a suitable way to prepare nanotubes, nanobelts, or nanoflakes of bismuth oxyiodide or other compounds with similar layered structures by means of appropriate control of the reaction parameters. We also believe that these distinctive nanostructures of bismuth oxychloride or oxybromide will expand their applications in the areas of photoluminescence, thermally stimulated conductivity, catalysts, and nanoscale devices.

Experimental Section

Materials: All chemicals used in this work, such as bismuth nitride ($Bi(NO_3)_3{\cdot}5H_2O$), NaOH, ethanol, CTAC, and CTAB, were of A.R. grade from the Beijing Chemical Factory (China) and were used without further purification.

Synthesis of bismuth oxyhalide nanobelts and nanotubes: $Bi(NO_3)_3{\cdot}5H_2O$ (0.5 g) and CTAB (0.5 g, to prepare bismuth oxybromide) or CTAC (0.5 g, to prepare bismuth oxychloride) were placed in distilled water at

room temperature. The mixture was stirred for ten minutes and the pH value of the resulting solution was adjusted to about pH 8–14 by addition of aqueous NaOH (6 M) solution. The solution was then stirred vigorously for 1 h and transferred into a Teflon-lined stainless steel autoclave (50 mL capacity). The autoclave was sealed and maintained at 120–180 °C for 2–24 h. After the reaction was completed, the resulting solid product was collected by filtration, then washed with deionized water and ethanol to remove any possible ionic species in the product, and then dried at 50 °C for 2 h.

Characterization: Powder X-ray diffraction (XRD) was performed on a Bruker D8-Advance X-ray powder diffractometer with $Cu_{K\alpha}$ radiation ($\lambda = 1.5418$ Å). The 2θ range used in the measurements was from 10 to 70° in steps of 0.02°. TEM images were taken by using a Hitachi model H-800 transmission electron microscope with an accelerating voltage of 200 kV. The structure and composition of the nanobelts were measured by high-resolution transmission electron microscopy (HRTEM, JEOL-2010F). Absorption measurements were carried out by using a Shimadzu UV-2100S spectrophotometer.

Acknowledgements

We thank Professor Joseph F. Chiang, Chairman of Chemistry and Biochemistry at the State University of New York (SUNY), Oneonta, for helpful discussions. This work was supported by the National Science Foundation of China (NSFC; 90406003, 20401010, 50372030, 20131030), the foundation for the authors of the National Excellent Doctoral Dissertation award of the P.R. China, and the state key project of fundamental research for nanomaterials and nanostructures (2003CB716901).

[1] a) X. F. Duan, C. M. Lieber, *Adv. Mater.* **2000**, *12*, 298–302; b) Y. Y. Wu, H. Q. Yan, M. Huang, B. Messer, J. H. Song, P. D. Yang P. D. Yang, *Chem. Eur. J.* **2002**, *8*, 1260–1268; c) B. Wiley, Y. G. Sun, B. Mayers, Y. N. Xia, *Chem. Eur. J.* **2005**, *11*, 454–463.

[2] a) D. W. Wang, Y. L. Chang, Q. Wang, J. Cao, D. B. Farmer, R. G. Gordon, H. J. Dai, *J. Am. Chem. Soc.* **2004**, *126*, 11602–11611; b) Y. J. Xiong, Y. Xie, Z. Q. Li, S. M. Gao, *Chem. Eur. J.* **2004**, *10*, 654–660; c) N. I. Kovtyukhova, T. E. Mallouk, *Chem. Eur. J.* **2002**, *8*, 4355–4363.

[3] a) R. Tenne, *Chem. Eur. J.* **2002**, *8*, 5297–5304; b) R. Gleiter, D. B. Werz, B. J. Rausch, *Chem. Eur. J.* **2003**, *9*, 2676–2683; c) C. H. Gorbitz, *Chem. Eur. J.* **2001**, *7*, 5153–5159.

[4] a) S. Iijima, *Nature* **1991**, *354*, 56–58; b) R. Tenne, L. Margulis, M. Genut, G. Hodes, *Nature* **1992**, *360*, 444–446; c) Y. Feldman, E. Wasserman, R. Tenne, D. J. Srolovitz, *Science* **1995**, *267*, 222–225; d) X. G. Peng, L. Manna, W. D. Yang, J. Wickham, E. Scher, A. Kadavanich, A. P. Alivisatos, *Nature* **2000**, *404*, 59–61; e) Y. G. Sun, Y. N. Xia, *Science* **2002**, *298*, 2176–2179; f) Z. P. Liu, J. B. Liang, S. Li, S. Peng, Y. T. Qian, *Chem. Eur. J.* **2004**, *10*, 634–640.

[5] a) Y. D. Li, J. W. Wang, Z. X. Deng, Y. Y. Wu, X. M. Sun, D. P. Yu, P. D. Yang, *J. Am. Chem. Soc.* **2001**, *123*, 9904–9905; b) J. W. Wang, Y. D. Li, *Adv. Mater.* **2003**, *15*, 445–447; c) Y. D. Li, X. L. Li, Z. X. Deng, B. C. Zhou, S. S. Fan, J. W. Wang, X. M. Sun, *Angew. Chem.* **2002**, *114*, 343–345; *Angew. Chem. Int. Ed.* **2002**, *41*, 333–335; d) Y. D. Li, X. L. Li, R. R. He, J. Zhu, Z. X. Deng, *J. Am. Chem. Soc.* **2002**, *124*, 1411–1416.

[6] a) X. Wang, Y. D. Li, *Chem. Eur. J.* **2003**, *9*, 300–306; b) X. Wang, Y. D. Li, *Chem. Eur. J.* **2003**, *9*, 5627–5635; c) J. F. Liu, Q. H. Li, T. H. Wang, D. P. Yu, Y. D. Li, *Angew. Chem.* **2004**, *116*, 5158–5162; *Angew. Chem. Int. Ed.* **2004**, *43*, 5048–5052; d) J. P. Ge, J. Wang, H. X. Zhang, X. Wang, Q. Peng, Y. D. Li, *Chem. Eur. J.* **2005**, *11*, 1189–1194; e) R. X. Yan, X. M. Sun, X. Wang, Q. Peng, Y. D. Li, *Chem. Eur. J.* **2005**, *11*, 2183–2195.

[7] a) W. P. Pan, Z. R. Dai, Z. L. Wang, *Science* **2001**, *291*, 1947–1949; b) J. J. Urban, W. S. Yun, Q. Gu, H. Park, *J. Am. Chem. Soc.* **2002**, *124*, 1186–1187; c) J. A. Nelson, M. J. Wagner, *J. Am. Chem. Soc.* **2003**, *125*, 332–333; d) M. E. Spahr, P. Bitterli, R. Nesper, M. Müller, F. Krumeich, H. U. Nissen, *Angew. Chem.* **1998**, *110*, 1339–1342; *Angew. Chem. Int. Ed.* **1998**, *37*, 1263–1265.

[8] a) J. J. Urban, W. S. Yun, Q. Gu, H. Park, *J. Am. Chem. Soc.* **2002**, *124*, 1186–1187; b) Y. P. Fang, A. W. Xu, R. Q. Song, H. X. Zhang, L. P. You, J. C. Yu, H. Q. Liu, *J. Am. Chem. Soc.* **2003**, *125*, 16025–16034; c) L. M. Qi, J. M. Ma, H. M. Cheng, Z. G. Zhao, *J. Phys. Chem. B* **1997**, *101*, 3460–3463; d) S. F. Chen, S. H. Yu, B. Yu, L. Ren, W. T. Yao, H. Colfen, *Chem. Eur. J.* **2004**, *10*, 218–223.

[9] a) N. Kijima, K. Matano, M. Saito, T. Oikawa, T. Konishi, H. Yasuda, T. Sato, Y. Yoshimura, *Appl. Catal. A* **2001**, *206*, 237–244; b) L. Y. Zhu, Y. Xie, X. W. Zheng, X. Yin, X. B. Tian, *Inorg. Chem.* **2002**, *41*, 4560–4566; c) T. M. Dellinger, P. V. Braun, *Scr. Mater.* **2001**, *44*, 1893–1897.

[10] J. T. Hu, T. W. Odom, C. M. Lieber, *Acc. Chem. Res.* **1999**, *32*, 435–445.

[11] J. W. Wang, Y. D. Li, *Chem. Commun.* **2003**, 2320–2321.

[12] a) J. Luo, S. L. Suib, *J. Phys. Chem. B* **1997**, *101*, 10403–10413; b) R. N. DeCuzman, Y. F. Shen, E. J. Neth, S. L. Suib, C. L. O'Young, S. Levine, J. M. Newsam, *Chem. Mater.* **1994**, *6*, 815–821; c) N. Kijima, H. Yasuda, T. Sato, Y. Yoshimura, *J. Solid State Chem.* **2001**, *159*, 94–102.

Received: May 16, 2005
Published online: August 10, 2005

